AD-A103 388 DEFECTS CONSTITUTIVE BEHAVIOR AND CONTINUUM TOUGHNESS 1/1
CONSIDERATIONS FOR WELD INTEGRITY ANALYSIS(U) NAVAL
RESEARCH LAB WASHINGTON DC P MATIC ET AL. 21 JUL 87
UNCLASSIFIED NRL-MR-5935 F/G 13/5 NL

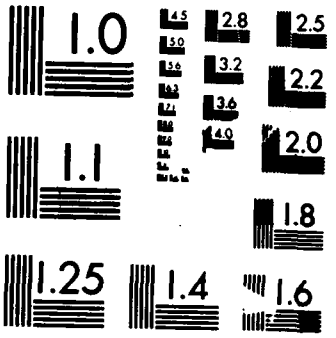

MICROCOPY RESOLUTION TEST CHART
NATIONAL BUREAU OF STANDARDS-1963-A

NRL Memorandum Report 5935

Defects, Constitutive Behavior and Continuum Toughness Considerations for Weld Integrity Analysis

PETER MATIC AND MITCHELL I. JOLLES

Mechanics of Materials Branch
Material Science and Technology Division

July 21, 1987

A183 229

SECURITY CLASSIFICATION OF THIS PAGE

REPORT DOCUMENTATION PAGE

1a. REPORT SECURITY CLASSIFICATION UNCLASSIFIED	1b. RESTRICTIVE MARKINGS
2a. SECURITY CLASSIFICATION AUTHORITY	3. DISTRIBUTION/AVAILABILITY OF REPORT Approved for public release; distribution unlimited.
2b. DECLASSIFICATION/DOWNGRADING SCHEDULE	
4. PERFORMING ORGANIZATION REPORT NUMBER(S) NRL Memorandum Report 5935	5. MONITORING ORGANIZATION REPORT NUMBER(S)
6a. NAME OF PERFORMING ORGANIZATION Naval Research Laboratory 6b. OFFICE SYMBOL (If applicable) Code 6382	7a. NAME OF MONITORING ORGANIZATION
6c. ADDRESS (City, State, and ZIP Code) Washington DC 20375-5000	7b. ADDRESS (City, State, and ZIP Code)
8a. NAME OF FUNDING/SPONSORING ORGANIZATION Office of Naval Research 8b. OFFICE SYMBOL (If applicable)	9. PROCUREMENT INSTRUMENT IDENTIFICATION NUMBER
8c. ADDRESS (City, State, and ZIP Code) Arlington, VA 22217	10. SOURCE OF FUNDING NUMBERS PROGRAM ELEMENT NO. 61153N; PROJECT NO; TASK NO. RR022-01-48; WORK UNIT ACCESSION NO. 480-509

11. TITLE (Include Security Classification)
Defects, Constitutive Behavior and Continuum Toughness Considerations for Weld Integrity Analysis

12. PERSONAL AUTHOR(S)
Matic, Peter and Jolles, Mitchell I.

13a. TYPE OF REPORT	13b. TIME COVERED	14. DATE OF REPORT (Year, Month, Day)	15. PAGE COUNT
Interim	FROM _____ TO _____	1987 July 21	23

16. SUPPLEMENTARY NOTATION

17. COSATI CODES			18. SUBJECT TERMS (Continue on reverse if necessary and identify by block number)
FIELD	GROUP	SUB-GROUP	Weld defects, Energy density, Fracture, True stress-true strain curve

19. ABSTRACT (Continue on reverse if necessary and identify by block number)

The failure load of a butt welded T-frame with a lack of fusion defect is predicted and compared with experimental data. Energy density concepts are used to quantitatively describe the material toughness at the continuum scale. Particular attention is given to the determination of base metal and weld metal uniaxial stress-strain curves valid for large deformation. Finite element results are used to predict the location where the energy density first reaches a critical value, and the corresponding applied load. The predicted initiation site and load compares favorably with the experiment.

20. DISTRIBUTION/AVAILABILITY OF ABSTRACT	21. ABSTRACT SECURITY CLASSIFICATION
☒ UNCLASSIFIED/UNLIMITED ☐ SAME AS RPT. ☐ DTIC USERS	UNCLASSIFIED
22a. NAME OF RESPONSIBLE INDIVIDUAL Peter Matic	22b. TELEPHONE (Include Area Code) (202) 767-5215
	22c. OFFICE SYMBOL Code 6382

DD FORM 1473, 84 MAR 83 APR edition may be used until exhausted
All other editions are obsolete

SECURITY CLASSIFICATION OF THIS PAGE

CONTENTS

DEFECTS, CONSTITUTIVE BEHAVIOR AND CONTINUUM TOUGHNESS CONSIDERATIONS FOR WELD INTEGRITY ANALYSIS

INTRODUCTION

The prediction of welded structural integrity is a problem complicated by geometry, inhomogeneous material composition and nonuniform deformation fields. Even in the best of circumstances, where optimum material quality and fabrication techniques are employed, integrity prediction must address these issues which are not present in many other types of structural problems. For these reasons, concepts of material and structural failure used to predict welded structural integrity should be formulated in terms of physical quantities and parameters which explicitly address and satisfy the analytical demands posed by welded structures.

The quantitative relationship between fabrication quality and welded structural integrity has yet to be determined in a manner sufficiently general to be used in the design process. Practical information can, of course, be obtained from weldment testing. If parameters used to describe weldment failure are sensitive to specimen size and geometry, however, the performance of a weldment cannot be used to reliably predict failure of a welded structure. Historically, this difficulty has been quite common.

The approach taken here is based on the explicit consideration of material fracture toughness at the continuum scale. At the continuum scale, the energy density required to produce material fracture is relatively insensitive to the particular degree of multiaxiality in the stress and strain states. Thus, size and geometry effects are avoided using an energy density material continuum fracture toughness definition. This further implies that crack tip fracture toughness parameters can, in principle, be determined from analyses using energy density concepts to predict test specimen behavior which is relevant for a particular structural size and geometry.

In this investigation, the application of energy density concepts is discussed and appropriate measures of continuum toughness are quantitatively defined. Interpretation of tension test data for a

Manuscript approved April 2, 1987

set of short arc welds is presented in a manner consistent with continuum plasticity and fracture toughness. Finite element analysis results for a welded T-section are presented. The predicted failure initiation load and location is shown to agree favorably with the experimentally observed failure load.

CONTINUUM MATERIAL TOUGHNESS CONCEPTS

A continuum volume of material undergoing deformation is characterized by its multiaxial stress state σ_{ij} and multiaxial strain state ϵ_{ij}. For ductile metals, which exhibit inelastic deformation, the strain state is a function of the stress state and stress history. The state of stress and strain may be related by a constitutive formulation which defines strain increments $d\epsilon_{ij}$ from the current stress state.

The strain energy per unit mass at a given instant during deformation, will be

$$w = \lim_{\Delta V \to 0} \left[\frac{1}{\rho} \frac{\Delta W}{\Delta V} \right] \tag{1}$$

$$= \int_0^{\epsilon_{ij}} \frac{\sigma_{ij}}{\rho} d\epsilon_{ij} \tag{2}$$

where ρ is the mass density. This energy density incorporates both stress and strain into a fundamental quantity relevant to thermodynamic descriptions of material deformation and damage. The energy density is a scalar quantity which takes into account all components of the stress and strain tensors in a physically consistent manner. Failure of the material, at the continuum scale, can be associated with the value of the energy density at which fracture occurs. Thus, the material toughness is defined as

$$w_c = \int_0^{(\epsilon_{ij})_c} \frac{\sigma_{ij}}{\rho} d\epsilon_{ij} \tag{3}$$

where w_c is the critical strain energy density value. The value of w_c, for engineering purposes, can be taken as a material constant. This makes w_c independent of the particular deformation state and is a unifying feature absent in failure criteria based on stress alone or strain alone.

For ductile metals, the material density varies only slightly, even over large deformations. For this reason, it is common to define an energy per unit volume density

$$w = \lim_{\Delta V \to 0} \left[\frac{\Delta W}{\Delta V} \right] \tag{4}$$

$$= \int_0^{\epsilon_{ij}} \sigma_{ij}\, d\epsilon_{ij}\,, \tag{5}$$

with an associated critical value

$$w_c = \int_0^{(\epsilon_{ij})_c} \sigma_{ij}\, d\epsilon_{ij}\,. \tag{6}$$

The energy per unit mass is fundamental, but the energy per unit volume is equally appropriate for constant volume deformation processes.

For the case of a uniaxial true stress-true strain curve, corresponding to a one-dimensional state of deformation, the critical energy density corresponds to the area under the uniaxial stress-strain curve, i.e.

$$w_c = \int_0^{\epsilon_c} \sigma d\epsilon \tag{7}$$

This representation is desirable for use with traditional constitutive formulations which rely on uniaxial stress-strain curves.

For a multiaxial state of stress, each of the six stress-strain pairs, three normal and three shear, must be evaluated and summed, i.e.

$$w_c = \int_0^{(\epsilon_{11})_c} \sigma_{11}\, d\epsilon_{11} + \int_0^{(\epsilon_{22})_c} \sigma_{22}\, d\epsilon_{22} + \int_0^{(\epsilon_{33})_c} \sigma_{33}\, d\epsilon_{33} + \tag{8}$$

$$+ \int_0^{(\epsilon_{12})_c} \sigma_{12}\, d\epsilon_{12} + \int_0^{(\epsilon_{23})_c} \sigma_{23}\, d\epsilon_{23} + \int_0^{(\epsilon_{31})_c} \sigma_{31}\, d\epsilon_{31}\,.$$

It should be noted that one or more individual terms in the multiaxial expression can be negative. Their total, w_c, must be positive, however.

A complete failure prediction should include the location of fracture initiation within the weld system and the value of the applied load at which failure occurs. No a priori selection of the fracture initiation site should be made. Each constituent material (i.e. base metal, weld metal and heat affected zones) is a candidate failure site. The continuum toughness of each constituent material can be determined from simple material tensile tests, and the results expressed in terms of the critical energy density value w_c for each constituent material.

A maximum value of the energy density will, in general, exist for each constituent material in a structure. A relative energy density ratio may be defined by dividing the energy density w, attained during the loading process, by the appropriate critical energy density, w_c. When values of this ratio are less than unity fracture initiation does not occur, i.e.

$$\left[\frac{w}{w_c}\right]_n < 1 \qquad n = 1, \ldots, N \tag{9}$$

where N is the total number of constituent materials in the structure.

As the load is increased, the structure will continue to deform. When the relative energy density ratio reaches unity at a site in one of the constituent materials, say n_c, so that

$$\left[\frac{w}{w_c}\right]_{n_c} = 1 \tag{10}$$

and

$$\left[\frac{w}{w_c}\right]_n < 1 \qquad n = 1, \ldots, n_c - 1, n_c + 1, \ldots, N \tag{11}$$

continuum fracture occurs in material n_c. By normalizing the energy density throughout the structure with the critical energy density for each material, the relative tendency for fracture to occur at different points in the structure can be quantified.

WELDED T-SECTION GEOMETRY

This investigation considers a welded T-section (Fig. 1) with flange and web thicknesses of 0.2''. The flange width was 2.0''. The web height was 1.8''. End plates were welded to the T-section to facilitate testing of the T-section in a tensile mode.

The weld line was located midway between the ends of the specimen. The weld itself was unsymmetrical, in the sense that the weld crowns on the top and bottom of the flange were offset. Radiography of the weld revealed a three-dimensional lack of fusion defect across the flange. The defect appeared to be offset with respect to the weld, along a line where the weld thickness was approximately that of the flange. Also, the defect appeared to span one-half of the flange thickness and have an out of plane dimension one-eighth of the flange thickness.

For the purposes of computational modeling, the weld crown was omitted from the model and the defect was located at the center of the weld material. This brought sufficient symmetry to the problem so that only one-quarter of the flange needed to be computationally modeled. The defect itself was idealized as a "slot-shaped" tunnel through the flange, with rounded ends (Fig. 2). This interpretation of the radiographic data was consistent with the location of the defect in the weld material and the geometry of the defect as known prior to the destructive testing of the specimen.

MATERIAL CHARACTERIZATION

Data from flat welded tensile specimens was available with which to characterize material behavior. The specimens were 0.2 in. thick base metal plates which had been welded together, in a similar manner as the T-section. They were cut into flat tensile specimens with the weld line spanning the specimen width.

The specimens tended to fracture in either the base metal adjacent to the weld metal, or in the weld metal itself. For the purposes of analysis, differentiation between base metal and weld metal behaviors were desired. No explicit treatment of the heat affected zone was made given the tensile specimen size and geometry. The occurrence of fractures in base metal adjacent to the weld included its effects, in an average sense, in the base metal characterization. Standard true stress-true strain curves were developed from specimen load-displacement data. The stress-strain curves exhibited significant scatter but no distinguishing trend between base metal failure and weld metal failure specimens (Fig. 3). The per cent reduction of area (%RA), however, while also exhibiting scatter, were clearly divided into two distinct groups of high %RA base metal failures and low %RA weld metal failures. The base metal failures fell into the range of 33.0 - 67.0 %RA. The weld metal failures fell into the range of 0.5 - 6.3 %RA.

The marked difference between base metal and weld metal ductility is not apparent from uniaxial considerations alone. Accurate assessments of the respective material toughness require an accurate uniaxial true stress-true strain representation. Such a representation should quantitatively reflect the

material ductility present in three-dimensional states of deformation. To accomplish this, continuum uniaxial true stress true-strain curves for the base metal and weld metal (Fig. 4) were generated using a procedure previously applied to ductile materials [1,2]. This procedure is based on results which suggest that the actual continuum uniaxial true stress-true strain curve will be more nonlinear than the calculated (or extrapolated) standard true stress-true strain curve over the full range of material deformation. This procedure was applied to a bilinear approximation of the averaged base metal and weld metal standard true stress-true strain curves.

The critical strain ϵ_c of the base metal at fracture was calculated based on the average base metal %RA since the base metal was essentially defect free and the %RA was influenced by weld geometry, some of which might enhance apparent base metal toughness, and some of which might degrade apparent base metal toughness.

The critical strain of the weld metal was calculated based on the maximum weld metal %RA, since the presence of defects in the weld metal would tend to reduce the apparent toughness. The maximum %RA served as a lower bound of the material toughness.

COMPUTATIONAL MODELING

The ABAQUS finite element code [3] was used for the analysis. The finite element grid is shown in Fig. 5. Symmetry considerations, as discussed above, required that only one quarter of the T-frame specimen be modeled. A total of 518 type C3D20H and C3D20 continuum elements were used. These are 20-noded elements with quadratic displacement interpolation. The C3D20H elements also include an independently interpolated linear hydrostatic stress. The hydrostatic stress is coupled to the constitutive relation using a Lagrange nultiplier. The use of such hybrid elements in regions of larger deformation near the defect prevented physically unrealistic displacement constraints from propagating through the grid. (Such constraints can lead to an artificially 'stiff' response of standard elements for incompressible or nearly incompressible deformations.)

Weld material uniaxial e stress-true strain behavior was assigned to elements in the denser portions of the finite element grid adjacent to the defect and to the elements of the web adjacent to the centerline. Base material behavior was assigned to the remainder of the model.

All analyses were performed with full geometric nonlinearity to account for large strains and large rotations. Rik's algorithm, which is load-displacement controlled, was used in the analysis to ensure numerical stability since the net load produced by the specimen deformation could decrease for large specimen elongations. In the absence of fracture initiation, this would correspond to the plastic limit load. Prediction of failure by this mode should not be precluded.

An incremental, rate independent plasticity theory was used for the material constitutive model [4]. Total strains in the multiaxial strain state ϵ_{ij} and uniaxial strain state ϵ are linearly decomposed into elastic and plastic components, i.e.,

$$\epsilon_{ij} = \epsilon_{ij}^{e} + \epsilon_{ij}^{p} \tag{12}$$

and

$$\epsilon = \epsilon^{e} + \epsilon^{p} . \tag{13}$$

The yield function f takes the form

$$f(\sigma_{ij}) = \sigma(\epsilon^{p}) \tag{14}$$

where σ_{ij} and σ are multiaxial and uniaxial stress states, respectively. The associated flow rule governs plastic strain increments by the relation

$$d\epsilon_{ij}^{p} = \lambda \frac{\partial f}{\partial \sigma_{ij}} . \tag{15}$$

In the case of purely elastic behavior $\lambda = 0$. For active yielding,

$$\lambda = d\epsilon^{p} \left(\frac{\sigma}{\sigma_{ij} \dfrac{\partial f}{\partial \sigma_{ij}}} \right) > 0 \tag{16}$$

Plastic strain increments also satisfy a dissipation equivalence condition

$$\sigma \, d\epsilon^{p} = \sigma_{ij} \, d\epsilon_{ij}^{p} \tag{17}$$

and a consistency condition

$$\frac{\partial f}{\partial \sigma_{ij}} d\sigma_{ij} - \frac{\partial \sigma}{\partial \epsilon^{p}} d\epsilon^{p} = 0. \tag{18}$$

The von Mises yield function

$$f(\sigma_{ij}) = \frac{3}{2} (s_{ij} s_{ij})^{1/2} \tag{19}$$

was employed. The deviatoric stress s_{ij} is defined as

$$s_{ij} = \sigma_{ij} - \frac{1}{3} \sigma_{kk} \sigma_{ij} . \tag{20}$$

where they hydrostatic component of stress is a $\sigma_{kk}/3$.

The finite element model of the T-section was loaded by displacements applied to the end of the specimen. A static analysis was performed. The ratio of energy density in the model to the local material toughness was calculated to be high at the center line of the T-section, adjacent to the weld defect in the weld metal. The element integration point for Element 1/Point 25 had the greatest energy density ratio. The energy density is plotted against the applied load for this point in Fig. 6. The energy density is initially very low, but as the material begins to deform in a nonlinear fashion the rate of change of energy density with respect to the applied load increases rapidly. The fracture of the Element 1/Point 25 was predicted to occur when the energy density, w, reaches the critical energy density, w_c, for the weld material. From this analysis, w reached the 4087 lb-in./in.^{3} toughness value for the weld metal at a predicted failure load of 30,500 lbs. The load-displacement response of the T-section predicted shows significant nonlinearity, in part due to yielding in both the base metal and weld metal (Fig. 7).

While the weld metal did exhibit nonlinearity in the stress-strain curve, its toughness value is relatively low as compared with the base metal toughness. It was assumed that once fracture initiation occurred, the resulting crack would propagate rapidly as the load bearing cross-section of the weld metal was reduced and the load redistributed itself over the as yet uncracked portion of the weld metal. For this reason, the predicted fracture initiation load was assumed to coincide with the failure load for the T-frame. Of course, if the weld material had sufficient toughness, stable crack growth would follow crack initiation and precede failure of the T-frame. Stable crack growth can be modeled, in principle, by the same concept, i.e., considering the local material toughness and the energy density in the crack tip region.

COMPARISON WITH EXPERIMENTAL RESULTS

As mentioned above, a laboratory test of the T-section was performed subsequent to the computational analysis. Conducted under structurally dynamic loading conditions, the test produced gross longitudinal strain rates of the order of 10^0 sec^{-1}. This global rate translated into local strain rates of 10^1 sec^{-1} in the vicinity of the defect. The local strain rate fell below the strain rate sensitivity threshold of 10^2 sec^{-1} for the weld metal and base metal, making the predicted failure load from the static analysis valid for comparison.

A T-section without a defect was tested to provide a reference load versus time response. Results for this test are shown in Fig. 8a. The specimen did not fracture under the applied load history. The load signal rises to a peak and subsequently oscillates as transducer ringing ensues.

The T-section with the flange defect was tested in an identical manner. The results are shown in Fig. 8b. The specimen fractured, and the onset of the event can be seen as a distinct drop in the load during the period from zero load to initial maximum load. The load signal increases after this drop and oscillation due to transducer ringing ensures. This signal is distinct from the defect free T-section. The fracture initiation load, coinciding with the first peak of the load history, was determined using the output from a strain gage mounted near the weld region. The strain gage output was related to load by a static calibration with the load transducer. The fracture initiation load of the T-section was 32,000 pounds and compared favorably with the predicted fracture initiation load of 30,5000 pounds obtained by the analysis.

SUMMARY

Material toughness at the continuum scale may be appropriately defined using the critical strain energy per unit mass at fracture. For constant volume processes, the critical strain energy per unit volume is equally appropriate. The value of this critical energy density can be determined from a simple material test. Three-dimensional aspects of the deformation and the corresponding influence on the energy density must be addressed. For uniaxial material test geometries, the standard true

stress-true strain curve developed from specimen load-displacement response is not an accurate description of the material constitutive response for large deformations leading to fracture. A more accurate continuum true stress-true strain curve can be developed from the uniaxial data and the per cent reduction of area.

The failure load of a welded T-section was predicted using this methodology. Radiographic examination of the T-section characterized a three-dimensional lack of fusion defect present in the weld material across the flange. A separate set of flat tensile coupons with transverse welds provided information on the constitutive behavior and continuum toughness of the base metal and weld metal. The predicted failure load, obtained from nonlinear finite element analysis, compared favorably with the failure load obtained from a laboratory test of the T-section performed subsequent to the numerical prediction.

The methodology discussed in this paper has been the basis for other studies on related types of weld integrity problems involving defect tolerance in large components [5], the influence of defects on the apparent toughness of weld metal tensile specimens [6] and weld system performance [7].

ACKNOWLEDGMENTS

The author wish to acknowledge the interest and support of Messrs. Peter M. Palermo and J. Allan Manuel and the Naval Sea Systems Command. The contributions of Dr. Frank J. Loss (Materials Engineering Associates, Inc.) and Mr. Jeffrey E. Beach (David Taylor Naval Ship Research and Development Center) to the experimental portion of this investigation is gratefully acknowledged.

REFERENCES

[1] Matic, P., "Numerically Predicting Ductile Material Behavior from Tensile Specimen Response," *Theoretical and Applied Fracture Mechanics*, Vol. 4, 1985, pp. 13-28.

[2] Matic, P., Kirby, G.C. III, Jolles, M.L., "The Relationship of Tensile Specimen Size and Geometry Effects to Unique Constitutive Parameters for Ductile Materials," submitted to *Proc. Roy. Soc.*

[3] ABAQUS User's Manual, Hibbitt, Karlsson and Soreson, Inc., Providence, RI, 1985 [Version 4.5 (a)].

[4] ABAQUS Theory Manual, Hibbitt, Karlsson and Sorenson, Inc., Providence, RI, 1984.

[5] Matic, P., Gensheimer, V.M., Jolles, M.I., "Integrity Analysis of a T-Frame Stiffened Panel with a Flange Weld Defect," to be published as NRL Memorandum Report 5990.

[6] Matic. P., Jolles, M.I., "The Influence of Small Defects on Tensile Specimen Ductility and Symmetry of Deformation," to be published as NRL Memorandum Report 5937.

[7] Matic, P., Jolles, M.I., "The Influence of Weld Metal Properties, Weld Geometry and Load on Weld System Performance," to be published as NRL Memorandum Report 5987.

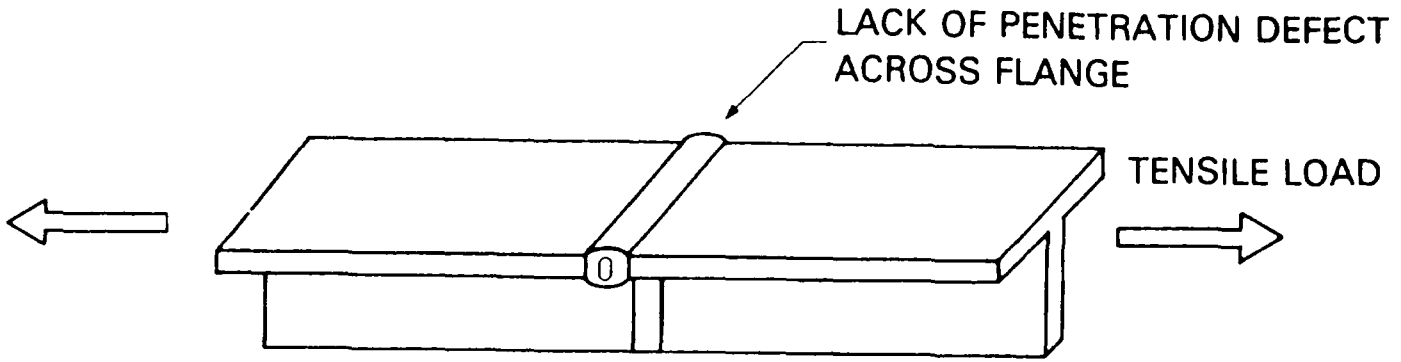

Fig. 1 — Welded T-frame

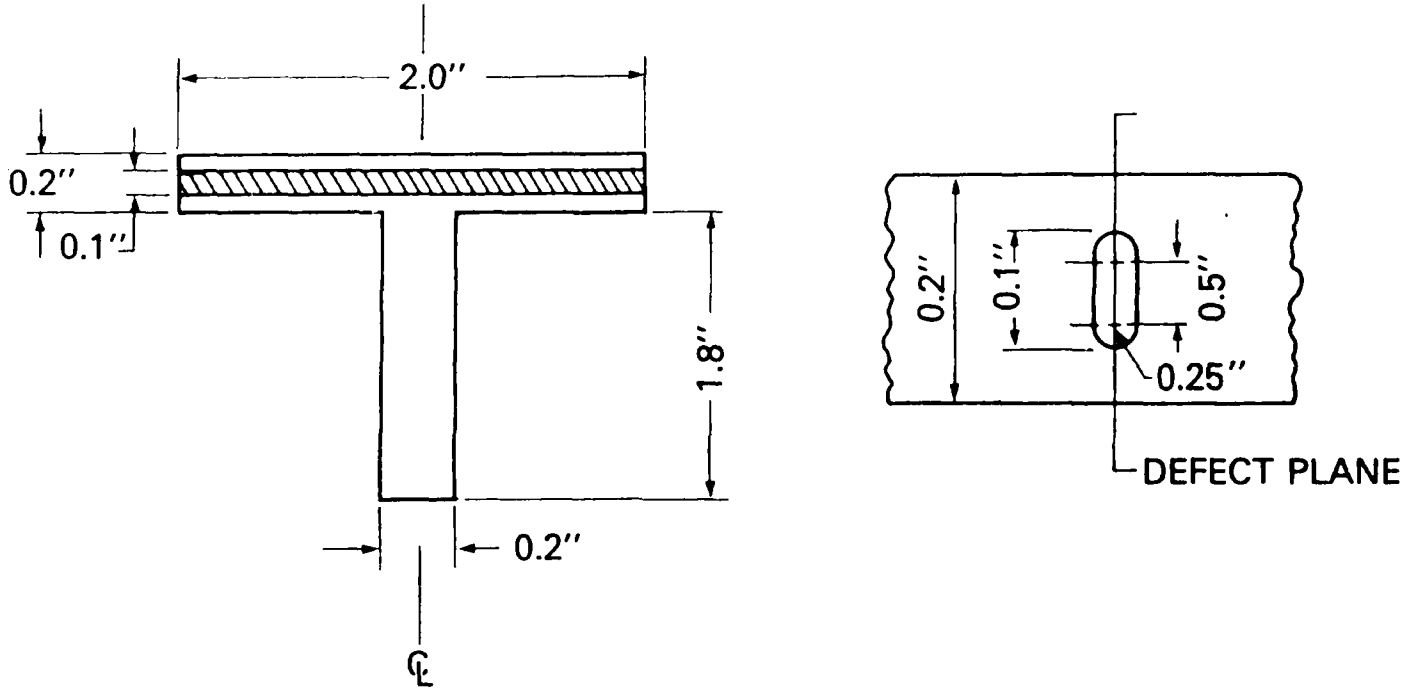

(a) CROSS SECTION AT DEFECT PLANE (b) DEFECT PROFILE THROUGH FLANGE

Fig. 2 -- T-frame and defect geometry

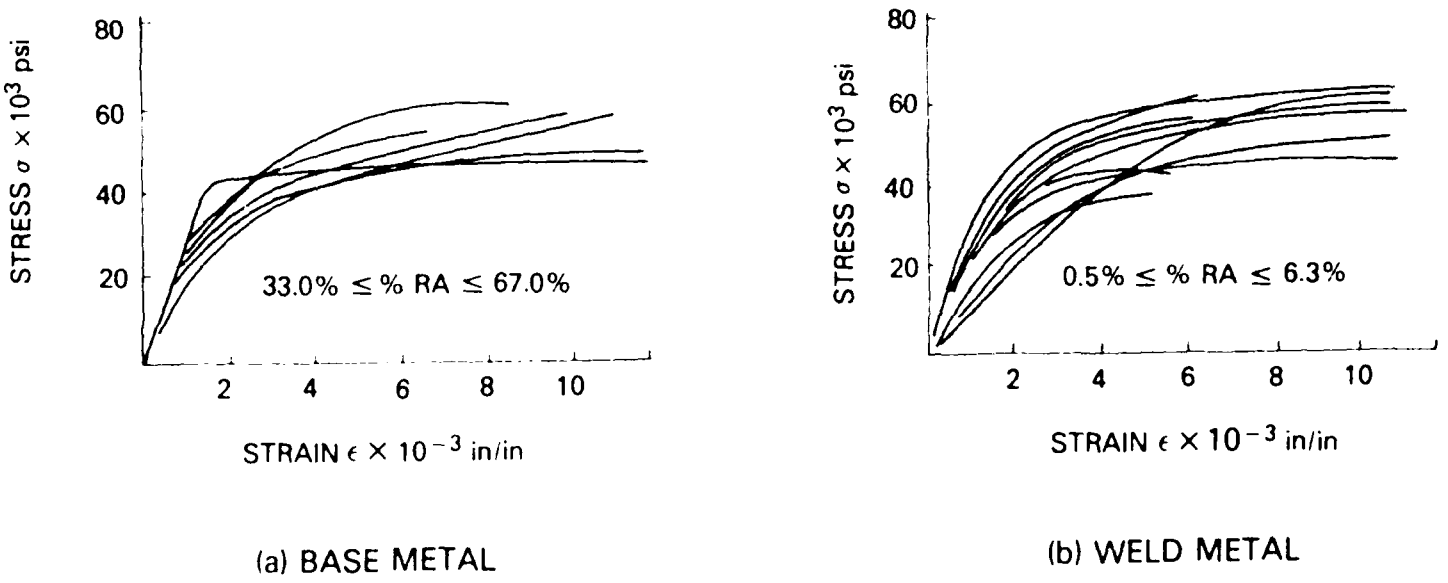

Fig. 3 — Standard true stress-true strain curves

BASE METAL

$\sigma_Y = 42.7 \times 10^3$ lb/in^2
$\epsilon_y = 0.00122$ in/in
$\sigma_c = 80.0 \times 10^3$ lb/in^2
$\epsilon_c = 0.680$ in/in
$w_c = 54023.$ lb in/in^3

WELD METAL

$\sigma_y = 49.2 \times 10^3$ lb/in^2
$\epsilon_y = 0.00153$ in/in
$\sigma_c = 63.4 \times 10^3$ lb/in^2
$\epsilon_c = 0.0662$ in/in
$w_c = 4087.$ lb in/in^3

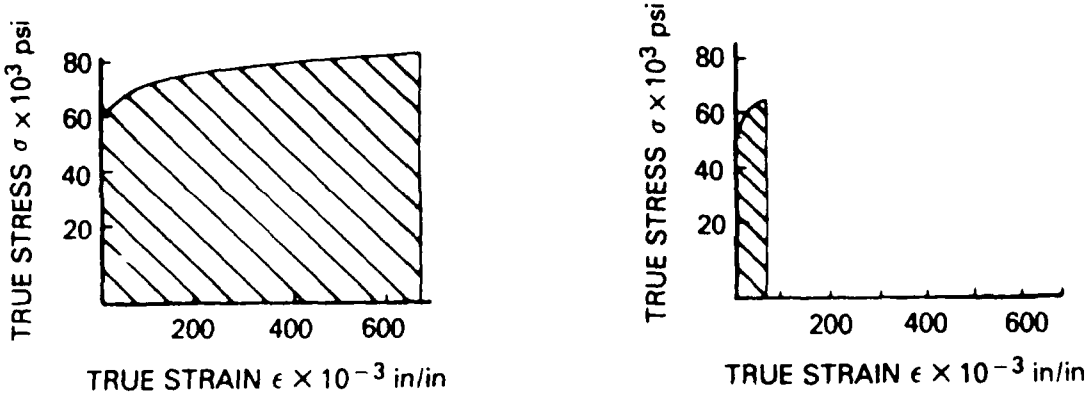

(a) BASE METAL
(HIGH PERCENT REDUCTION OF AREA)

(b) WELD METAL
(LOW PER CENT REDUCTION OF AREA)

Fig. 4 — Continuum true stress-true strain curves

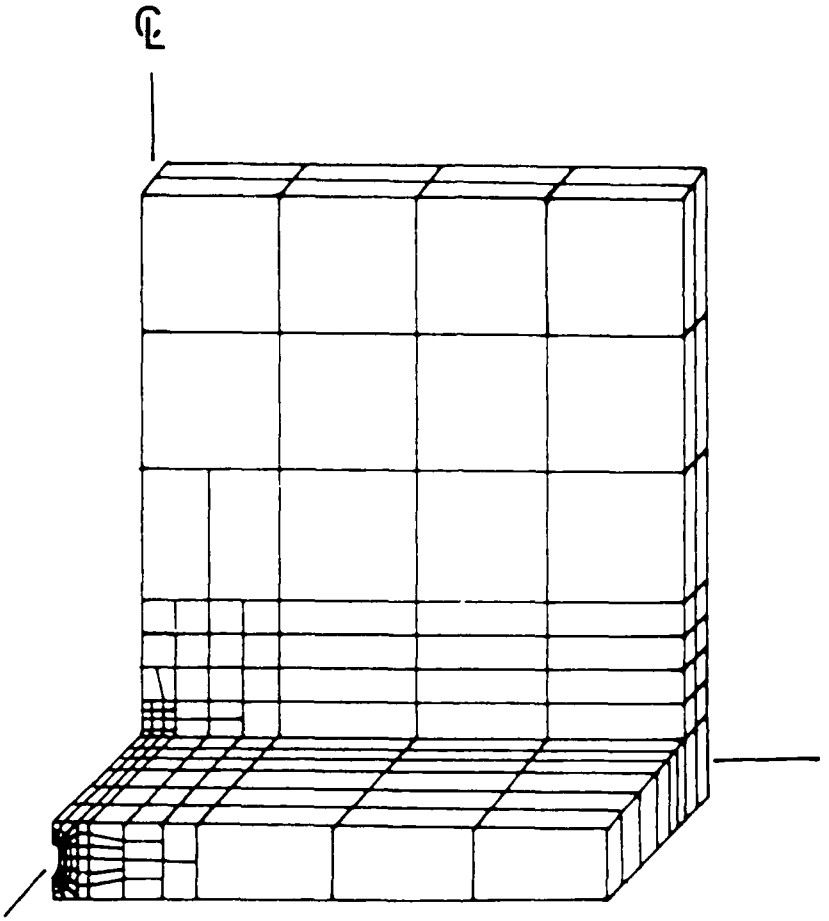

Fig. 5 — Finite element model

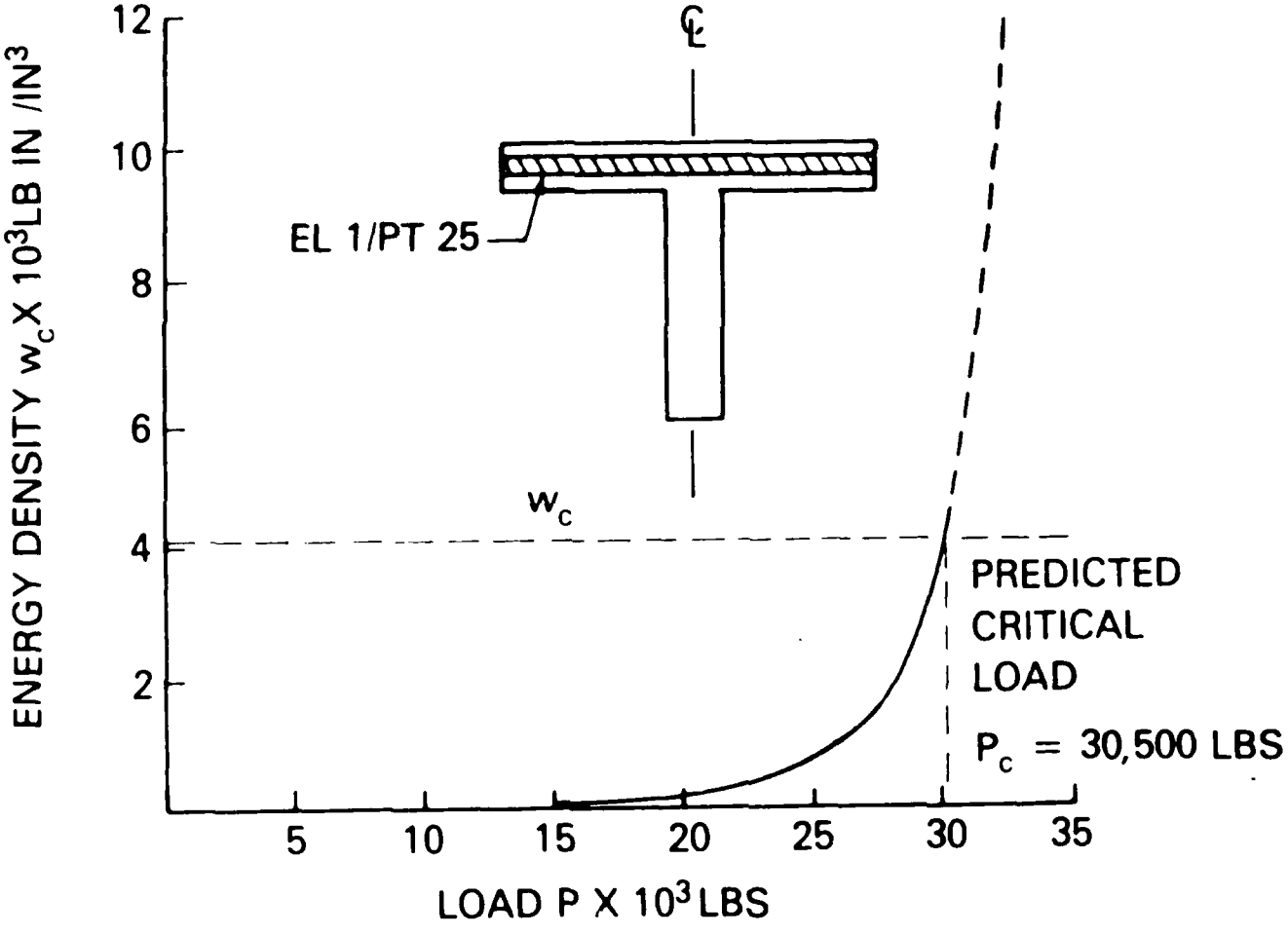

Fig. 6 — Energy density vs applied load at element 1/point 25 of finite element model

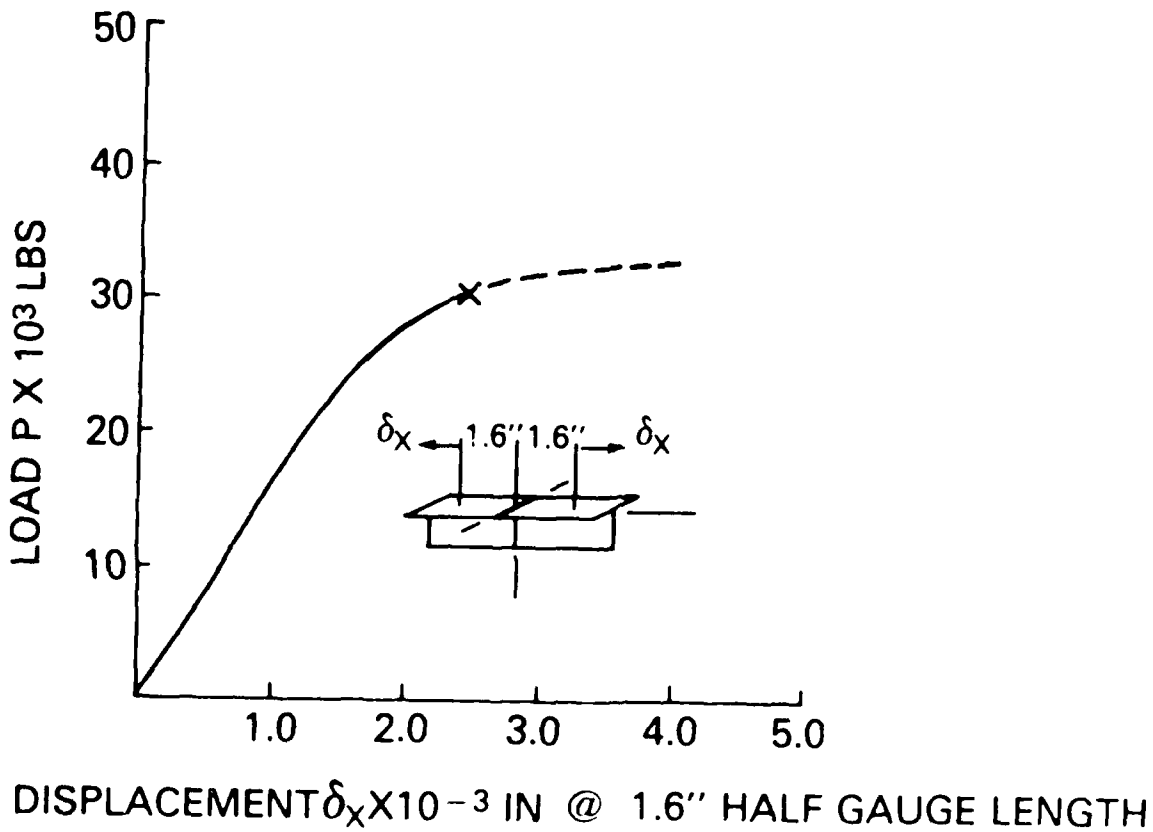

Fig. 7 — Predicted T-frame load—displacement plot from finite element results

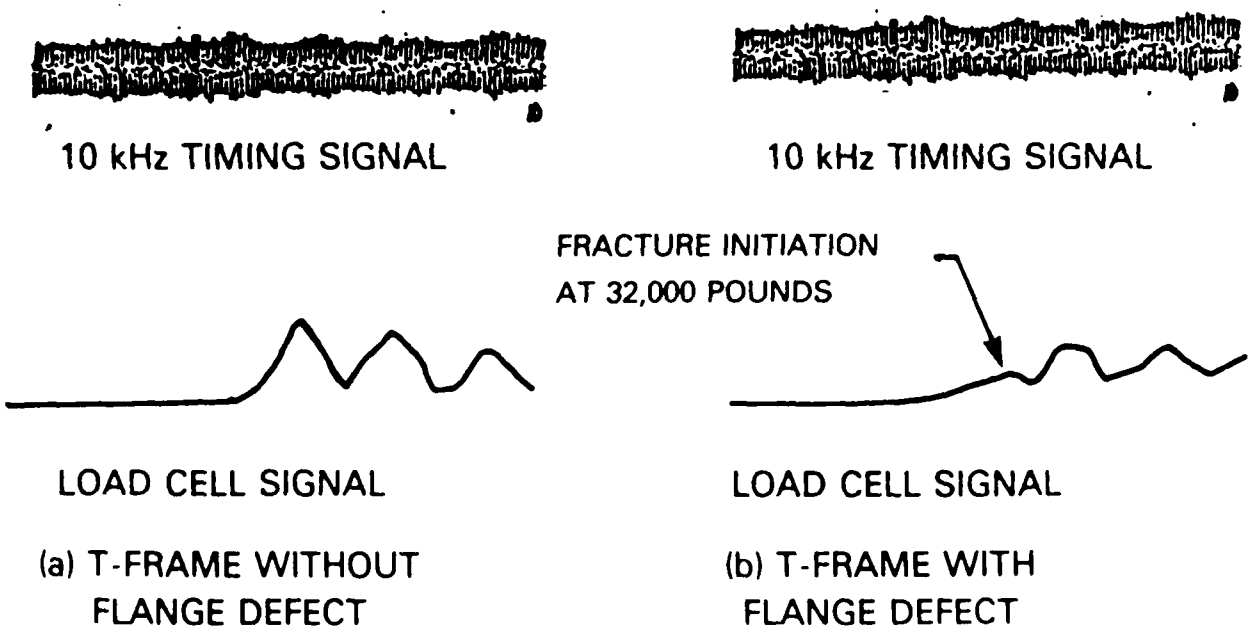

Fig. 8 — T-frame data from laboratory tests

END

9-87

DTIC